

Fine-structure intervals and polarizabilities of highly excited *p* and *d* states of sodium*

T. F. Gallagher, L. M. Humphrey, R. M. Hill, W. E. Cooke, and S. A. Edelstein

Molecular Physics Center, Stanford Research Institute, Menlo Park, California 94025

(Received 4 November 1976)

Selective field ionization of the $|m_j|$ fine-structure levels of highly excited *p* and *d* states of Na has been used to measure the fine-structure (fs) intervals and tensor polarizabilities of the *p* states from $n = 16$ to 19 and *d* states from $n = 15$ to 17 by rf spectroscopy. Using a two-step photo-excitation scheme we selectively excite one fs state of a *p* or *d* level and set the ionizing field so that it will field ionize the other fs state but not the one pumped by the lasers. Consequently, as the rf frequency is swept through the fs resonance, a substantial increase in the ionization current is observed. Our measurements show that the *p* fs intervals follow an $(n^*)^{-3}$ rather than an n^{-3} scaling law (n^* is the effective principal quantum number). The polarizabilities of both *p* and *d* states are in good agreement with calculations using a Coulomb approximation. The measurements of the *d*-state polarizabilities now cover a wide enough range of n to confirm the theoretical prediction of an n^7 scaling law.

I. INTRODUCTION

Highly excited sodium atoms are interesting for several reasons. On the one hand, sodium is a simple, one-electron system. As such it has many properties such as polarizabilities and radiative lifetimes which depend on purely electronic wave functions that can be calculated with some confidence using adaptations of hydrogenic wave functions.¹ On the other hand, some of the finer details of the spectra such as the fine-structure intervals of the *p* and *d* states are completely different from hydrogen due to the effects of the Na⁺ core which are not as yet well understood.

The recent development of the tunable dye laser has made possible the efficient production of Rydberg states of sodium which has stimulated the development of a variety of experimental techniques for both the production and detection of highly excited atoms.²⁻⁴ We report here a novel laser excitation-selective ionization technique which we have used to make radio-frequency resonance measurements of fine-structure intervals and polarizabilities of a series of highly excited *p* and *d* states of sodium.

Earlier measurements of *p*-state fine-structure intervals, made by high-resolution optical spectroscopy, extend only up to $n=9$.⁵ Recently, Ducas and Zimmerman⁶ have used the Stark effect to shift the Na 10s-17*p* transition frequency into resonance with a CO₂ laser line to derive a value for the 17*p* fine-structure interval. Recently, Harvey *et al.* have measured the fine-structure interval and polarizabilities of the sodium 4*d* state by two-photon spectroscopy.⁴ The fine-structure (fs) intervals of the $n=9$ to 16 *d* states and the polarizabilities of the 10 to 12 *d* states have been measured by Haroche *et al.* using quantum beat spectroscopy.^{2,7,8} Using a microwave resonance tech-

nique, we have measured the *d*-state fine-structure intervals from $n=11$ to 16.⁹ A recent study of the Stark effect in Na by Littman *et al.*¹⁰ is, of course, related to these polarizability measurements.

II. THEORY

The Hamiltonian for the energy levels of the sodium atom in a weak electric field E can be written as¹¹

$$\mathcal{H} = \mathcal{H}_{\text{Coul}} + \mathcal{H}_{\text{fs}} - \alpha_0 E^2 - \alpha_2 E^2 \frac{3m_l^2 - J(J+1)}{J(2J-1)}. \quad (1)$$

$\mathcal{H}_{\text{Coul}}$ represents the Coulomb interaction of the valence electron with the ionic core. The energy W of each principal series of l is given (in atomic units) by

$$W = -1/2n^{*2}, \quad (2)$$

where $n^* = n - \delta_l$ and δ_l is the quantum defect of the l state. As a result of the different quantum defects, l states of the same n are not degenerate but have different energies as shown by Fig. 1. \mathcal{H}_{fs} represents the spin-orbit coupling which is strongly affected by the penetration of the Na⁺ core by the valence electron. The $\alpha_0 E^2$ and $\alpha_2 E^2$ terms are the leading terms in the perturbation

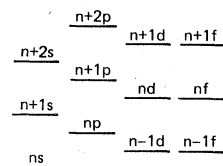


FIG. 1. Energy levels of sodium showing the relative positions of *s*, *p*, *d*, and *f* states. Although it is difficult to discern on this scale, the *nd* state lies slightly below the *nf* state.

expansion for the Stark effect (in even powers of E). Such an expansion may be used to express the energy of a state only for fields weak enough that the state's Stark shift is much less than the energy separation from adjacent l states, a condition which is met in our experiments. At fields somewhat below where the perturbation expansion becomes invalid, the higher-order E^4 and E^6 terms in the Stark effect begin to appear. α_0 and α_2 are, respectively, the scalar and tensor polarizabilities which characterize the second-order Stark shift. α_0 describes the common displacement of all the m_j states of a given J , and α_2 determines the splitting of the m_j levels. In Eq. (1) we have neglected the effect of hyperfine structure which is negligible in our experiments.¹²

Khadjavi *et al.*¹¹ have derived general expressions for the polarizabilities α_0 and α_2 which depend on angular factors in the form of 6- J symbols and the energy differences and radial matrix elements between states coupled by the electric field. Their results can be simplified by assuming that the radial matrix elements for the different fine-structure states of the same l are the same and that the fine-structure splittings are small compared to the Δl energy separations. The polarizabilities $\alpha_0(J)$ and $\alpha_2(J)$ of the np_J and nd_J states (in atomic units) then become

np states

$$\alpha_0(\frac{1}{2}) = \alpha_0(\frac{3}{2}) = -\frac{2}{9}S - \frac{4}{9}D, \quad (3a)$$

$$\alpha_2(\frac{1}{2}) = 0, \quad (3b)$$

$$\alpha_2(\frac{3}{2}) = \frac{2}{9}S + \frac{2}{45}D; \quad (3c)$$

nd states

$$\alpha_0(\frac{3}{2}) = \alpha_0(\frac{5}{2}) = -\frac{4}{15}P - \frac{2}{5}F, \quad (4a)$$

$$\frac{10}{7}\alpha_2(\frac{3}{2}) = \alpha_2(\frac{5}{2}) = \frac{4}{15}P + \frac{4}{35}F. \quad (4b)$$

Here

$$\begin{aligned} S &= \sum_{n'} \frac{|\int R(np)R(n's)r dr|^2}{E_{np} - E_{n's}}, \\ D &= \sum_{n'} \frac{|\int R(np)R(n'd)r dr|^2}{E_{np} - E_{n'd}}, \\ P &= \sum_{n'} \frac{|\int R(nd)R(n'p)r dr|^2}{E_{nd} - E_{n'p}}, \\ F &= \sum_{n'} \frac{|\int R(nd)R(n'f)r dr|^2}{E_{nd} - E_{n'f}}, \end{aligned} \quad (5)$$

where $R(nl)$ is the radial wave function and E_{n_l} the energy of the n_l state. Note that in both the p and d states, the scalar polarizabilities of both J levels are equal and that the d -state tensor polarizabilities are related by the factor of $\frac{10}{7}$. It can be seen that our assumptions are justified by comparing

the prediction for d states that $\alpha_0(\frac{3}{2}) = \alpha_0(\frac{5}{2})$ and $\frac{10}{7}\alpha_2(\frac{3}{2}) = \alpha_2(\frac{5}{2})$ with experimental results. The measurements of Harvey *et al.*⁴ show that for the $4d$ state of Na $\alpha_0(\frac{3}{2})$ and $\alpha_0(\frac{5}{2})$ differ by less than 1% and that $\frac{10}{7}\alpha_2(\frac{3}{2})$ is equal to $\alpha_2(\frac{5}{2})$ to within 3%.

Taking advantage of the relation between the polarizabilities of the fine-structure states shown in Eqs. (3) and (4), we may rewrite the polarizabilities to eliminate the J subscript in the following way:

np states

$$\alpha_0(p) = \alpha_0(\frac{1}{2}) = \alpha_0(\frac{3}{2}), \quad (6)$$

$$\alpha_2(p) = \alpha_2(\frac{3}{2});$$

nd states

$$\alpha_0(d) = \alpha_0(\frac{3}{2}) = \alpha_0(\frac{5}{2}), \quad (7)$$

$$\alpha_2(d) = \frac{10}{7}\alpha_2(\frac{3}{2}) = \alpha_2(\frac{5}{2}).$$

The sums S and D , P and F of Eq. (5) are dominated by the contributions of states nearest in energy to the np and nd states, respectively. The nearby states have the largest radial matrix elements and the smallest energy denominators. If we consider only the closest states in each sum, we can at least determine the signs of the polarizabilities. From the energy level diagram of Fig. 1 we see that the np state lies just above the $n-1$ d state and about midway between the ns and $n+1$ s states so that we expect that $S \sim 0$, $D > 0$, and that $\alpha_0(p) < 0$ and $\alpha_2(p) > 0$. The nd state lies just below the nf state and the $n+1$ p state so that we would expect that $P < 0$, $F < 0$, and $\alpha_0(d) > 0$ and $\alpha_2(d) < 0$. This is in agreement with our intuitive expectation from second-order perturbation theory that in an electric field the d -state energy will decrease and the p -state energy will increase due to repulsion from the nearby levels to which they are coupled by the electric field.

Assuming these values for the signs of the polarizabilities, we can construct the energy level diagrams of Fig. 2 showing the behavior of the $|m_j|$ levels in an electric field. The vertical lines show the $\Delta m = 0$, $\Delta J = \pm 1$ transitions which we observe in our experiments. The frequencies $\nu_{l, |m_j|}$ of the three transitions can be derived from Eqs. (1), (6), and (7) to be

$$\begin{aligned} \nu_{p, 1/2} &= S_p + \alpha_2(p)E^2/2, \\ \nu_{d, 3/2} &= S_d + \alpha_2(d)E^2/20, \\ \nu_{d, 5/2} &= S_d + 9\alpha_2(d)E^2/20, \end{aligned} \quad (8)$$

where S_p and S_d are the fine-structure intervals of the p and d states. Note that the expressions of Eq. (8) do not contain $\alpha_0(p)$ or $\alpha_0(d)$.

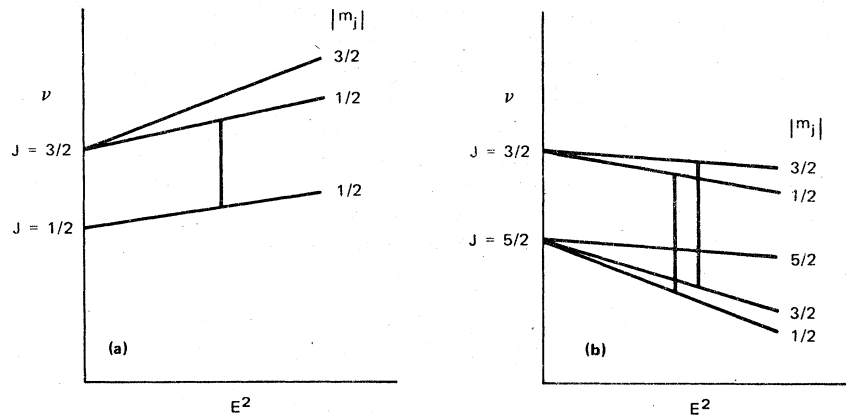


FIG. 2. Energy level diagrams of (a) the p -state fine-structure $|m_j|$ levels and (b) the d -state fine-structure $|m_j|$ levels in an electric field. The observed $\Delta m = 0$ transitions are shown by the vertical lines.

III. EXPERIMENTAL METHOD

The basic idea of the experiment is illustrated by Fig. 3 which shows the relevant energy levels for a resonance experiment with the Na $16d$ state. Using two pulsed tunable dye lasers pumped by the same N_2 laser, we excite the sodium atoms in an atomic beam from the ground $3s_{1/2}$ state to the $3p_{1/2}$ state and then to the $16d_{3/2}$ state. 1–2 μsec after the laser excitation we apply a pulsed electric field which is strong enough to ionize only the $16d_{5/2}$ state but not the $16d_{3/2}$ state; consequently, there is usually no ionization signal. If we apply a radio-frequency (rf) field during the time between the laser pulses and the ionizing pulse, then as we sweep the frequency of the rf field through the $d_{3/2}$ - $d_{5/2}$ fine-structure transition frequency, we see a large increase in the ionization signal as shown in Fig. 4.

The ability to selectively populate and ionize the fine-structure states is crucial to the method. Selective population is achieved by choosing the

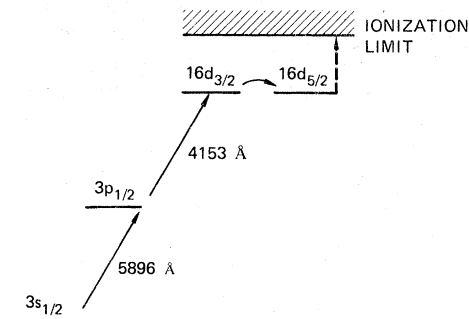


FIG. 3. Relevant energy levels for the resonance experiment on the $16d$ state. The single arrows indicate the two-step laser pumping of the $16d_{3/2}$ state; the curved arrow indicates the radio-frequency fine-structure transition; and the broken arrow indicates the selective ionization of the $16d_{5/2}$ state by the electric field.

$3p_{1/2}$ or $3p_{3/2}$ state as the intermediate state in the laser pumping to take advantage of the $\Delta J = 0, \pm 1$ selection rule. If we use the $3p_{1/2}$ state, we can populate only the $nd_{3/2}$ states. Using the $3p_{3/2}$ state, we populate predominantly the $nd_{5/2}$ state because the $\Delta J = 1$ transition is stronger than the $\Delta J = 0$ transition. To populate the p states, we must apply a small electric field of 10–100 V/cm to mix states of even parity with the higher p states. The polarizability calculations show the principal admixtures to the $np_{1/2}$ and $np_{3/2}$ states are the $n-1 d_{3/2}$ and $n-1 d_{5/2}$ states, respectively. Consequently, by using $3p_{1/2}$ and $3p_{3/2}$ as intermediate states in the laser pumping, we can selectively populate the $np_{1/2}$ and $np_{3/2}$ states, respectively.

To understand the selective ionization of the fine-structure states, we must recall that the

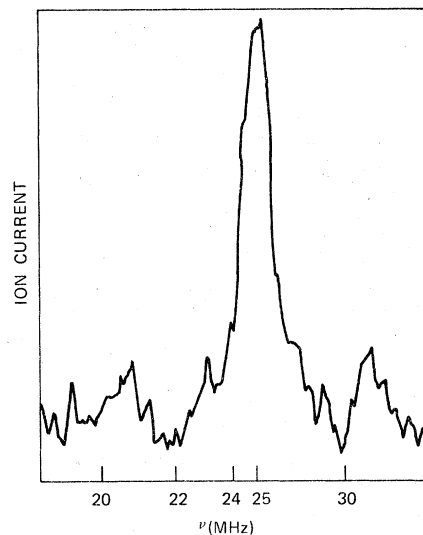


FIG. 4. $16d, \frac{3}{2}$ resonance in an external field of 1.34 V/cm taken on a sweep of increasing frequency.

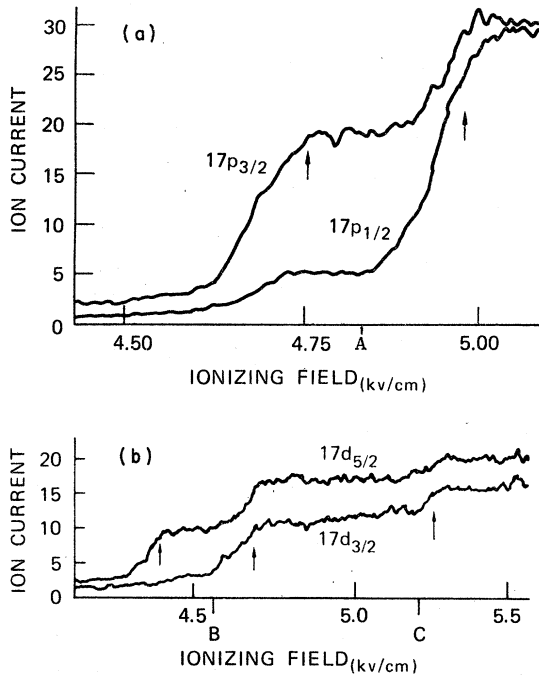


FIG. 5. Experimental traces of ionization current vs ionizing field for (a) the $17p_{1/2}$ and $17p_{3/2}$ states, and (b) $17d_{3/2}$ and $17d_{5/2}$ states with the approximate locations of the ionization thresholds indicated by arrows. A, B, and C indicate the ionization fields used for the resonance experiments on these states.

ionizing pulse is $\sim 0.2 \mu\text{sec}$ long.¹³ Consequently we observe ionization of a state when the field is strong enough that the state's ionization rate is $\geq 10^7 \text{ sec}^{-1}$. If we plot the ionization current vs ionizing electric field, we see a threshold field for the ionization of each state, corresponding to an ionization rate of 10^7 sec^{-1} . In Fig. 5 we show the experimental plots of the ionization thresholds for the $17p_{1/2}$, $17p_{3/2}$, $17d_{3/2}$ and $17d_{5/2}$ states (J states were selectively populated by the proper choice of the intermediate $3p$ state). The approximate locations of the ionization thresholds are indicated by the arrows. The assignment of $|m_j|$ values to the thresholds is done by correlating the low-field $|m_j|$ states with the high-field $|m_l|$ states to which they are adiabatically connected. Since the explanation of how the assignments are made is given in Refs. 13 and 14, we only present the assignments here.

The low-field $|m_j|$ values and high-field $|m_l|$ values assigned to the thresholds are given in Table I. As shown by Table I states of the same $|m_j|$ but different J have different ionization thresholds since they correlate to different high-field $|m_l|$ states. Note that for the $17p_{3/2}$ state the $|m_j| = \frac{1}{2}$ state has a lower ionization threshold than the

$17p_{1/2}$ state. Likewise, for the $17d_{5/2}$ state both the $|m_j| = \frac{1}{2}$ and $\frac{3}{2}$ states have lower ionization thresholds than for the $17d_{3/2}$ state. It is the difference in the ionization thresholds for states of the same $|m_j|$ but different J which makes these resonance experiments possible. Note that the $17p_{1/2}$ state shows the vestige of a threshold at the same ionizing field as the $J = \frac{3}{2}, |m_j| = \frac{1}{2}$ state which we attribute to the breakdown of the ΔJ selection rules in the dc electric field.

To explain the details of the resonance method it is convenient to label the states as $l, |m_j|$ and the transitions as $l, |m_j|$ (since the transitions are $\Delta J \pm 1, \Delta m_j = 0$). Let us consider the example of the $n = 17, p, \frac{1}{2}$ transition. We initially populate the $p_{1/2, 1/2}$ state. If the ionizing field is set to point A of Fig. 5, then only the $p_{3/2, 1/2}$ level will be ionized. As the frequency of the rf is swept through the $p, \frac{1}{2}$ resonance, the atoms undergo transitions to the $p_{3/2, 1/2}$ state from which they are ionized by the electric field, producing a sharp increase in the observed ion current as shown in Fig. 6. The $d, \frac{1}{2}$ and $d, \frac{3}{2}$ transitions can be observed in a similar manner by setting the ionizing field to points B and C of Fig. 5(b), respectively. Although there is appreciable background ionization of the $d_{3/2, 1/2}$ state for the $d, \frac{3}{2}$ resonance, it is still quite obvious as shown in Fig. 4.

All the experiments were done using the electric resonance method first used by Hughes.¹⁵ Although $d \rightarrow d$ and $p \rightarrow p$ are not allowed electric dipole transitions if we apply a small dc field to admix a small amount of states of opposite parity, then we can use an rf electric field to drive the transitions. For the p and d states we used dc fields of up to 100 and 4 V/cm, respectively. At these fields J is not a "good" number, and the ΔJ selection rules for the laser excitation breakdown. We chose to use electric resonance rather than mag-

TABLE I. Threshold fields for the ionization of $17p$ and $17d |m_j|$ states.

	J	State $ m_j $	m_l	Threshold field (kV/cm)
$17p$	$\frac{3}{2}$	$\frac{1}{2}$	1	4.87
	$\frac{3}{2}$	$\frac{3}{2}$	0	4.70
	$\frac{1}{2}$	$\frac{1}{2}$	1	4.87
$17d$	$\frac{5}{2}$	$\frac{1}{2}$	0	4.36
	$\frac{5}{2}$	$\frac{3}{2}$	1	4.63
	$\frac{3}{2}$	$\frac{1}{2}$	1	4.63
	$\frac{5}{2}$	$\frac{5}{2}$	2	5.17
	$\frac{3}{2}$	$\frac{3}{2}$	2	5.17

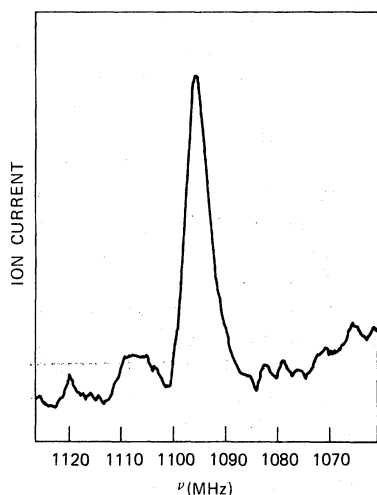


FIG. 6. $18p, \frac{1}{2}$ resonance in an external field of 35.6 V/cm taken on a sweep of increasing frequency.

netic resonance mainly because it is technically easier due to the lower power requirements.

The laser-atomic-beam apparatus for these measurements is similar to those used by Ducas *et al.*³ and Stebbings *et al.*¹⁶ and is described in detail elsewhere¹⁴ so we shall only briefly outline its basic features here. As shown by Fig. 7 an atomic sodium beam passes between a plate and a grid 1.12 cm apart, where it is crossed by the two laser beams. A positive high-voltage pulse is applied to plate *b* ionizing the highly excited Na atoms and accelerating the ions through the grid into the electron multiplier. The ion signal from the multiplier, a current burst ~50 nsec wide,

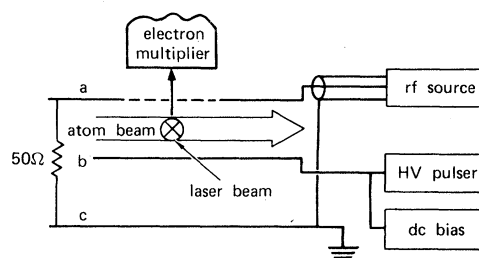


FIG. 7. Interaction region. The atomic beam is crossed by the laser beams (shown going into the paper) between grid *a* and plate *b*. The high-voltage ionizing pulse is applied to plate *b* which ionizes the atoms and accelerates the ions through the grid and into the electron multiplier. The rf is introduced by a 50- Ω coaxial cable which is terminated by a 50- Ω resistor between grid *a* and grounded plate *c*.

goes to a boxcar averager, the output of which is recorded on a chart recorder. The rf electric field is applied to the plates with a 50- Ω coaxial cable as shown in Fig. 7. The 50- Ω shunt resistor terminates the coaxial line to avoid power fluctuations due to resonances in the transmission line. Since the dc bias voltage is also applied to the plates, the dc and rf electric fields are parallel and only $\Delta m_j = 0$ rf transitions are allowed.

Data were taken by sweeping the rf frequency through the resonance in both directions to cancel offsets produced by the time constant of the boxcar averager. The 20 to 35 MHz frequencies of the *d* transitions were generated with a Hewlett Packard 606A signal generator and measured with a Systron Donner 512 counter. These frequencies were measured with an accuracy of ± 0.2 MHz.

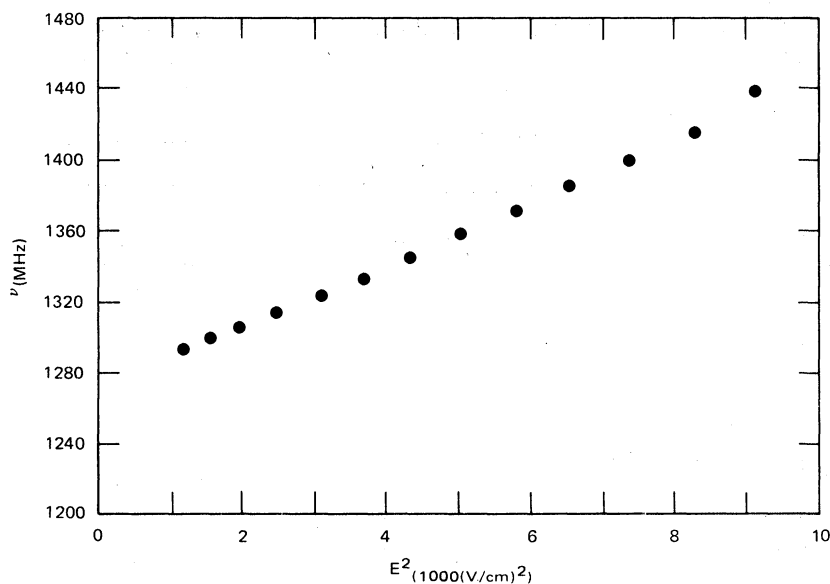


FIG. 8. Frequency of the $17p, \frac{1}{2}$ transition vs E^2 . Note that the frequency does not have linear dependence on E^2 .

TABLE II. *p*-state fine-structure intervals and polarizabilities.

<i>n</i>	S_0 (MHz)	α_2 [10^{-2} MHz/(V/cm) ²]	<i>C</i> [10^{-7} MHz/(V/cm) ⁴]	$\alpha_2(\text{calc})$ [10^{-2} MHz/(V/cm) ²]	$\alpha_0(\text{calc})$ [MHz/(V/cm) ²]
16	1548.7(20)	2.2(2)	0.17	1.98	-0.224
17	1279.2(25)	3.2(3)	0.78	3.13	-0.349
18	1068.4(15)	5.0(4)	2.21	4.90	-0.542
19	902.9(15)	7.4(8)	5.90	7.41	-0.809

The frequencies of the *p* transitions, in the range from 900 to 1600 MHz, were provided by a Hewlett Packard 1814A signal generator. We measured these frequencies by directing 1% of the rf power through a wavemeter to a crystal detector and recording the output of the detector on the second pen of the chart recorder used to record the ionization signal. On each frequency scan we set the wavemeter twice, once below and once above the atomic resonance, producing dips in the rf power trace at the two wavemeter settings. For frequencies above 1 GHz we used a Hewlett-Packard 536A wavemeter and for frequencies below 1 GHz we used a Polytechnic 587A wavemeter. Both wavemeters were calibrated using a Hewlett-Packard 5340A microwave counter. The accuracy of our frequency measurements using this procedure was ± 0.2 MHz.

IV. RESULTS

For the *p* resonances, data were taken at various dc electric fields from 10 to 100 V/cm and the transition frequencies were plotted vs E^2 as shown in Fig. 8. From Fig. 8 it is quite apparent that the data do not fit the simple linear form of Eq. (8), and that higher-order terms must be included to fit the data. Accordingly we first fit the observed frequencies to a power series in E^2 including terms up to E^6 . The coefficients of the E^6 term changed sign for different values of *n* which seemed unphysical; thus we chose to keep terms only to E^4 and fit the observed frequencies ν to the power series

$$\nu = S_p + \frac{1}{2}\alpha_2 E^2 + CE^4. \quad (9)$$

Here, it is apparent that the constant term is the

fine-structure interval S_p and that the E^2 coefficient is half the tensor polarizability. The E^4 coefficient *C* can be related to the hyperpolarizability.¹⁷ The values of the constants S_p , α_2 , and *C* obtained from the fits of Eq. (9) to the data are given in Table II. The uncertainties given in Table II are typically one third larger than the differences between the values obtained for the fitted constants with and without the E^6 term. This is in fact the largest uncertainty in the experiment. Also given in Table II are the values of α_0 and α_2 calculated using the Coulomb approximation of Bates and Damgaard¹ to evaluate the radial matrix elements.

In the *d*-state measurements we obtained similar frequency vs field squared plots, an example of which is shown in Fig. 9. Both the $d, \frac{3}{2}$ and $d, \frac{1}{2}$ transition frequencies were extrapolated to zero field to obtain the fine-structure interval, but only the $d, \frac{3}{2}$ frequencies were used to obtain the polarizability because the Stark shift of the $d, \frac{3}{2}$ transition is nine times as large as that of the $d, \frac{1}{2}$ transition. The results of the measurements are presented in Table III with the calculated values of α_0 and α_2 .

Our measurement of the 17*p* fine-structure interval agrees with the value 1245(50) MHz obtained by Ducas and Zimmerman.⁶ The *p* fine-structure intervals are a valuable extension of the previous measurements enabling us to determine the scaling law for the *p* fine-structure interval quite accurately. In Fig. 10 we have plotted S_p/n^{*3} and S_p/n^3 , and it is quite apparent that S_p varies as $1/n^{*3}$ not $1/n^3$.

As shown by Table III, the *d*-state fine-structure intervals reported here are in good agreement with the values obtained by quantum beat spectroscopy⁸ and microwave spectroscopy.⁹

These measurements of the *d*-state polarizabil-

TABLE III. *d*-state fine-structure intervals and polarizabilities.

<i>n</i>	S_d^a (MHz)	S_d^b (MHz)	S_d (MHz)	α_2 [MHz/(V/cm) ²]	$\alpha_2(\text{calc})$ [MHz/(V/cm) ²]	$\alpha_0(\text{calc})$ [MHz/(V/cm) ²]
15	-28.0(10)	-26.1(10)	-28.6(10)	-1.06(15)	-0.94	2.95
16	-23.0(10)	-25.0(9)	-24.0(10)	-1.47(20)	-1.49	4.71
17			-19.8(10)	-2.78(40)	-2.29	7.17

^aSee Ref. 7.^bSee Ref. 9.

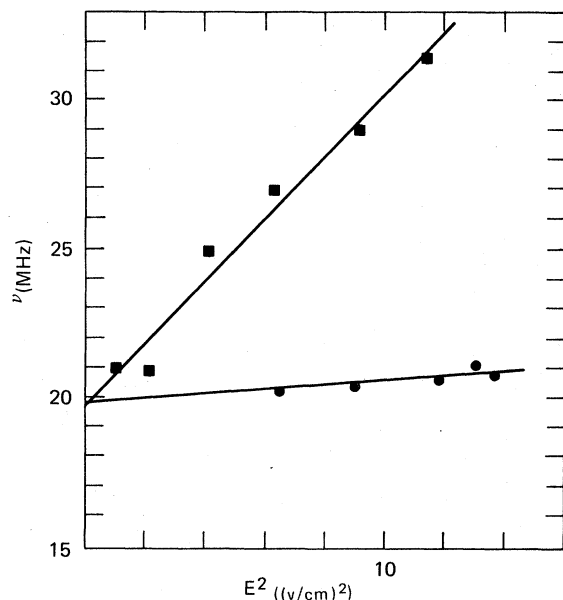


FIG. 9. Frequencies of the $17d, \frac{1}{2}$ (●) and $17d, \frac{3}{2}$ (■) transitions vs E^2 .

ities extend the range of the measurements to include the d states from $n=4$ to $n=17$, making a good test of the expected n^7 scaling possible. Using the results of these experiments and those of Ref. 8, we have plotted α_2/n^6 , α_2/n^7 , and α_2/n^8 vs n in Fig. 10. Although there is considerable scatter in the experimental data, it is clear that α_2/n^7 is constant and that α_2/n^6 and α_2/n^8 are not, confirming the n^7 scaling law.

The calculated and observed values of α_2 given

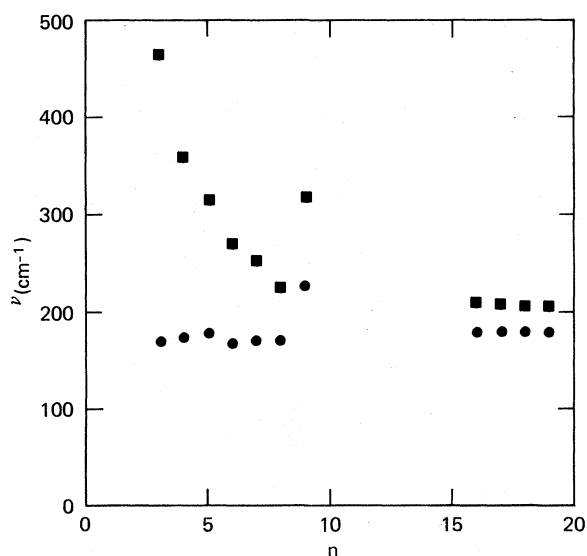


FIG. 10. Plot of $n^3 S_p$ vs n (■) and $n^3 S_p$ vs n (●) showing the $(1/n^*)^3$ scaling of S_p .

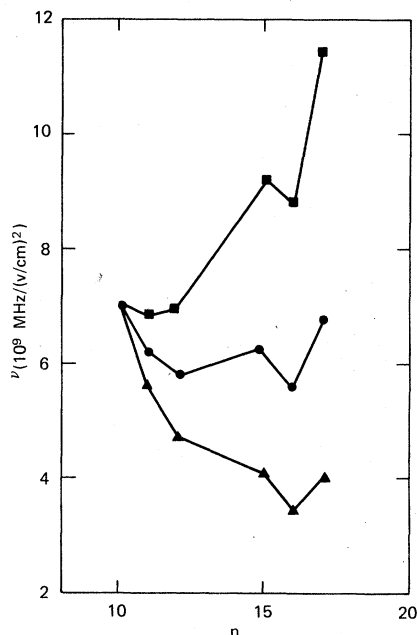


FIG. 11. Plots of $0.1 \alpha_2/n^6$ (■), α_2/n^7 (●), and $10 \alpha_2/n^8$ (▲) vs n for the Na d states showing the n^7 dependence of α_2 for $n > 10$.

in Tables I and II are in agreement, which gives us confidence that the calculated values for α_0 are equally accurate. The calculations show that for the nd state, $\sim 75\%$ of α_2 is due to the nf state and $\sim 20\%$ to the $n+1 p$ state. For the np state, the dominant contribution to α_2 is from the $n-1 d$ state. The net effect of the nearly cancelling ns and $n+1$ states is to reduce α_2 by 10% from the value calculated using the $n-1 d$ state alone.

We hope that these measurements of fine-structure intervals and polarizabilities will stimulate renewed theoretical interest both in understanding the effects of the core on the fine-structure interaction and in developing new approximate techniques for calculating electronic properties of Rydberg states. We are confident that the experimental method presented here will be useful in future studies of highly excited states. The method is simple and efficient and can be refined in countless ways to achieve greater sensitivity and accuracy.

ACKNOWLEDGMENTS

We would like to acknowledge helpful discussions with G. W. Series and S. Svanberg in the course of this work. We are grateful to M. Zimmerman for providing us with his computer program for calculating the radial matrix elements. We would also like to thank J. Watgen, U. Gysel, W. Bischel, and G. Tomlin for the generous loans of rf equipment.

- *This work supported by the Electric Power Research Institute.
- ¹D. R. Bates and A. Damgaard, *Phil. Trans. Roy. Soc. London* 242, 101 (1949).
- ²S. Haroche, M. Gross, and M. P. Silverman, *Phys. Rev. Lett.* 33, 1063 (1974).
- ³T. W. Ducas, M. G. Littman, R. R. Freeman, and D. Kleppner, *Phys. Rev. Lett.* 35, 366 (1975).
- ⁴K. C. Harvey, R. T. Hawkins, G. Meisel, and A. L. Schawlow, *Phys. Rev. Lett.* 34, 1073 (1975).
- ⁵C. E. Moore, *Atomic Energy Levels*, NBS Circ. No. 467 (U.S. GPO, Washington, D.C., 1949).
- ⁶T. W. Ducas and M. Zimmerman (unpublished).
- ⁷C. M. Fabre, M. Gröss, and S. Haroche, *Opt. Commun.* 13, 393 (1975).
- ⁸C. M. Fabre and S. Haroche, *Opt. Commun.* 15, 254 (1975).
- ⁹T. F. Gallagher, R. M. Hill, and S. A. Edelstein, *Phys. Rev. A* 13, 1448 (1976).
- ¹⁰M. G. Littman, M. L. Zimmerman, T. W. Ducas, R. R. Freeman, and D. Kleppner, *Phys. Rev. Lett.* 35, 366 (1975).
- ¹¹A. Khadjavi, A. Lurio, and W. Happer, *Phys. Rev.* 167, 128 (1968).
- ¹²H. Kopferman, *Nuclear Moments* (Academic, New York, 1958).
- ¹³T. F. Gallagher, L. M. Humphrey, R. M. Hill, and S. A. Edelstein, *Phys. Rev. Lett.* 37, 1465 (1976).
- ¹⁴T. F. Gallagher, L. M. Humphrey, W. E. Cooke, R. M. Hill, and S. A. Edelstein (unpublished).
- ¹⁵H. K. Hughes, *Phys. Rev.* 72, 614 (1947).
- ¹⁶R. F. Stebbings, C. J. Latimer, W. P. West, F. B. Dunning, and T. B. Cook, *Phys. Rev. A* 12, 1453 (1975).
- ¹⁷A. D. Buckingham, *Advances in Chemical Physics* (Interscience, New York, 1967), Vol. 12, p. 107.